Calculation of Stress Trajectories Using Fracture Mechanics

BO DOWSWELL

ABSTRACT

In structures composed of plates and plate-like elements subjected to in-plane stresses, the stress flow around discontinuities is an important design consideration. Stress dispersion angles are used extensively in gusset plate design and calculations for web local yielding of wide flange members. The current design values are empirical, and the variables affecting the dispersion angles are not well understood. Due to the wide range of angles published in the literature, an analytical model that accounts for all variables is necessary for full understanding of the behavior of these elements. Using fracture mechanics principles, this paper shows that the dispersion angle is dependent on geometry, constraint and inelastic deformation capacity. A versatile design procedure, which explicitly accounts for all variables affecting the stress dispersion angle, is presented.

Keywords: gusset plates, stress flow, discontinuities, fracture mechanics.

INTRODUCTION

In structures composed of plates and plate-like elements subjected to in-plane stresses, the stress flow around discontinuities is an important design consideration. A common discontinuity in steel-frame structures occurs where a concentrated load is dispersed into an element over a finite length. In a typical vertical brace connection, shown in Figure 1a, the brace axial load is dispersed into the gusset plate over the length of the brace-to-gusset connection. Another discontinuity is shown in Figure 1b, where the axial load in the post is transferred into the girder. To calculate the local strength of the girder web, the angle of dispersion within the girder must be estimated. The dispersion angle around openings in plate and shell structures must also be accurately predicted in order to calculate the proper development length of reinforcement and to estimate the net area at an offset group of openings.

The existing literature contains a wide range of experimental dispersion angles based on test results and finite element models. Researchers have reported angles as low as 16.1° and as high as 74°. Current design recommendations are limited to angles between 15° and 71.6°.

Due to the wide range of dispersion angles published in the literature, an analytical model that accounts for all of the variables affecting the stress dispersion angle is necessary for full understanding of the behavior of these elements. It will be shown that the dispersion angle is dependent on geometry, constraint and inelastic deformation capacity. This paper presents a versatile design solution, derived from the principles of fracture mechanics, that explicitly accounts for all variables affecting the stress dispersion angle.

Bo Dowswell, P.E., Ph.D., Principal, SDS Resources, LLC, Birmingham, AL. E-mail: bo@sdsresources.com

CURRENT DESIGN RECOMMENDATIONS

Design recommendations can be found in specifications, manuals, books and journal papers. In design, stress dispersion angles are used to determine an effective width of the element, where only a portion of the element is active in resisting the load.

Gusset Plates

For design, AISC (2011) treats gusset plates as rectangular, axially loaded members with a cross-sectional area $L_w t$, where L_w is the Whitmore width, and t is the plate thickness. The Whitmore width is calculated by assuming the stress spreads through the gusset plate at an angle of 30°. Whitmore widths are shown in Figure 2 for various connection configurations.

Web Local Yielding

This section discusses the local strength of members at concentrated loads located at the flanges and acting in the plane of the web. According to the AISC *Specification* (AISC, 2010) Section J10.2.a, web local yielding occurs when the web material adjacent to the fillet yields under a tensile or compressive force. When the concentrated force is applied at a distance from the member end greater than the depth of the member, the nominal load is

$$R_n = F_{yw}\, t_w \left(5k + l_b\right) \quad (1)$$

where

F_{yw} = specified minimum yield stress of the web, ksi
k = distance from outer face of flange to the web toe of the fillet, in.
l_b = length of bearing, in.
t_w = thickness of web, in.

The 2010 AISC *Specification* equations are based on a 2.5-to-1 slope from the load application point to the fillet as shown in Figure 3, which is a 68.2° dispersion angle. Eurocode (2005) Sections 6.2.6.2 and 6.2.6.3 have similar requirements, which are also based on a 68.2° dispersion angle.

For web yielding at end plate moment connections Eurocode (2005) specifies a 45° dispersion angle through the weld and the end plate and a 68.2° dispersion angle (2.5-to-1 slope) through the column flange and fillet radius. AISC Steel Design Guide 4 (Murray and Sumner, 2003) recommends a 45° dispersion angle through the weld and the end plate and a 71.6° dispersion angle (3-to-1 slope) through the column flange and fillet radius.

Plate and Shell Structures

Support points and openings for plate and shell structures are often reinforced with stiffening elements to prevent local

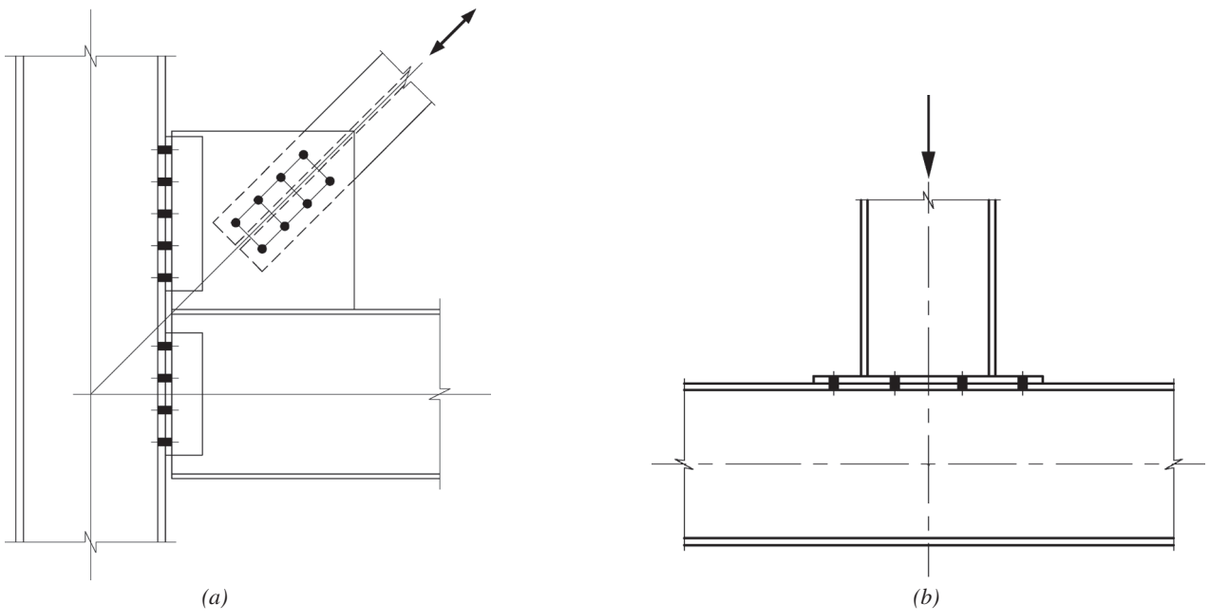

Fig. 1. Common discontinuities in steel-frame structures: (a) vertical brace connection; (b) post-to-girder connection.

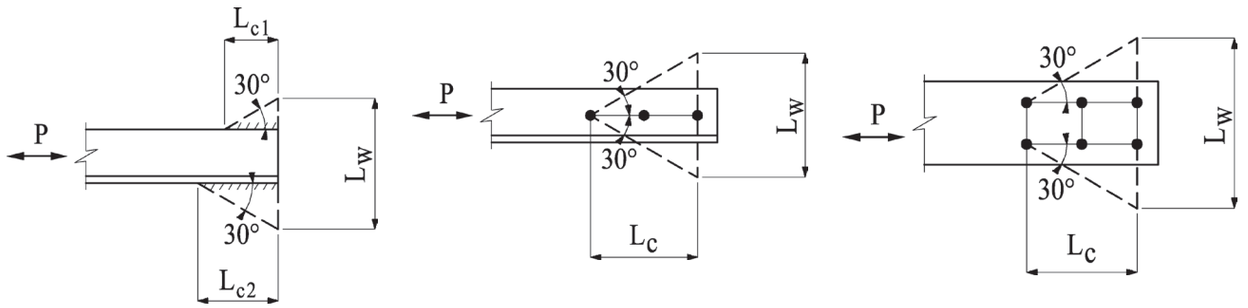

Fig. 2. Effective widths for various connection configurations.

yielding or buckling. The dispersion angle around openings must be accurately predicted in order to calculate the proper development length of reinforcement and to estimate the net area at an offset group of openings. Support members attached to the shell, such as the silo support in Figure 4, must be designed to properly disperse the stress into the shell to avoid buckling.

ASME *Steel Stack Code* (ASME, 2001) Section 4.6.1 states, "The top and bottom of the breeching opening shall be adequately reinforced to transfer the discontinuities of shell stress back to the full circumference of the shell." According to Commentary 5 of the CICIND *Model Code for Steel Chimneys* (CICIND, 1999), "Vertical reinforcement should be continued above and below the opening to a point where the added stress is unimportant. The code deems that continuing the reinforcement beyond horizontal stiffeners above and below the opening a distance at least 0.5 times the width of the opening will suffice." This implies a dispersion angle, θ, of 45° as shown in Figure 5.

Wolf (1983) discussed the design of silos at materials handling plants, and cited the transfer of load from the silo wall to the support columns as the most common cause of failure in these structures. He recommended that the loads be spread through the shell at an angle of 45°.

At locations of concentrated loads on steel tanks, Wozniak (1990) assumes the load to spread at an angle of 30° on each side of the stiffener as shown in Figure 6. The stiffener length is extended to a point where the stress in the shell is less than the allowable buckling stress. Wozniak also recommends that reinforcement be extended beyond openings far enough to allow a stress dispersion into the shell of 30°. Kaups and Lieb (1986) made similar recommendations for bins and silos.

For design of oil tanker structures with "several openings located in or adjacent to the same cross section," ABS (2009) Sections 2.6.3.6 and 2.6.3.8 specify an equivalent opening size based on a shadow area. The shadow area is calculated using "two tangent lines with an angle of 15 degrees to the longitudinal axis of the ship," as shown in Figure 7.

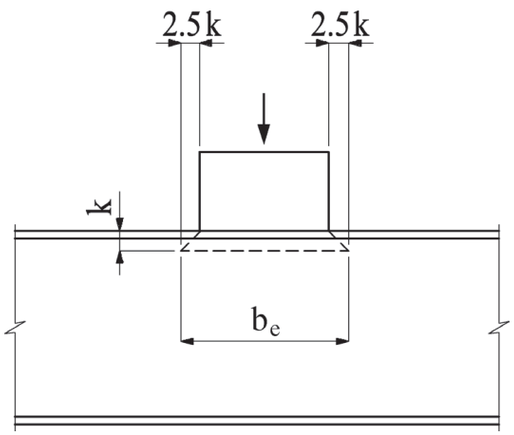

Fig. 3. Web local yielding.

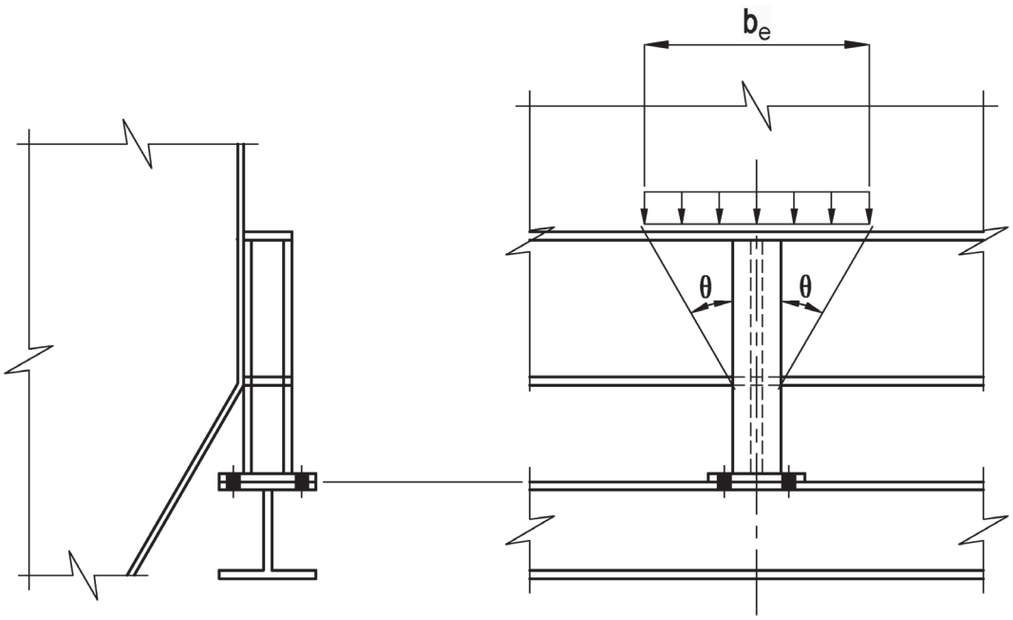

Fig. 4. Attachment to shell at discretely supported silo.

Connections

Owens and Cheal (1989) recommended dispersion angles of 30°, 45° and 68° for various conditions at steel connections, depending on the ductility of the fitting, boundary conditions and local symmetry.

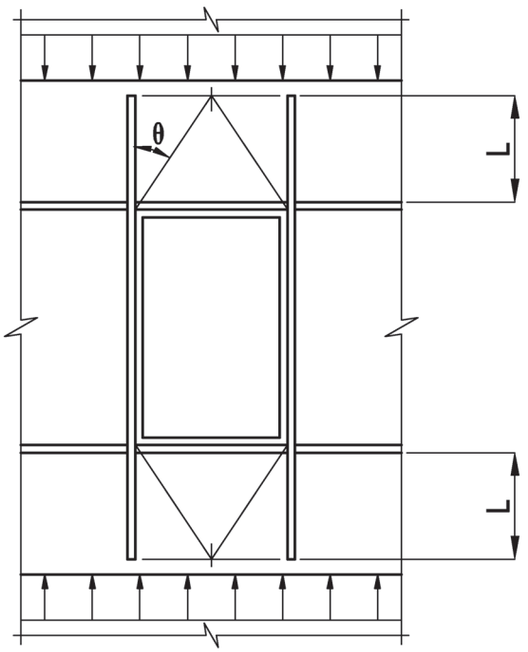

Fig. 5. Reinforced breech opening in a stack.

Crane Girders

The vertical normal stress in the web of a crane girder can be calculated by assuming that the wheel load disperses through the rail and top flange at an assumed angle, as shown in Figure 8. Ricker (1982) suggested an angle of 60°; however, a more conservative value of 45° has been adopted in CMAA (1994) Section 3.3.2.3, AS (2001) Section 5.7.3.3 and AISE (1997) Section 5.8.6.

EXISTING RESEARCH

Gusset Plates

The first major experimental work on gusset plates was done by Wyss (1923). The stress trajectories were plotted for gusset plate specimens representing a warren truss joint. The maximum normal stress was at the end of the brace member. Wyss noted that the stress trajectories were along approximately 30° lines with the connected member.

Sandel (1950) conducted a photoelastic stress analysis of a 1/22-scale model of a Warren truss joint. The stress trajectories are shown in Figure 9a. He concluded that the normal stress at the end of the bracing members can be calculated more accurately using a stress trajectory angle of 35° instead of the 30° suggested by Wyss.

Whitmore (1952) tested 1/8-in.-thick aluminum gusset plates with a yield strength of 39 ksi and a modulus of elasticity of 10,000 ksi. The specimen was a 4-scale model of a Warren truss joint with double gusset plates. Data from strain gages mounted on the gusset plates were used to plot

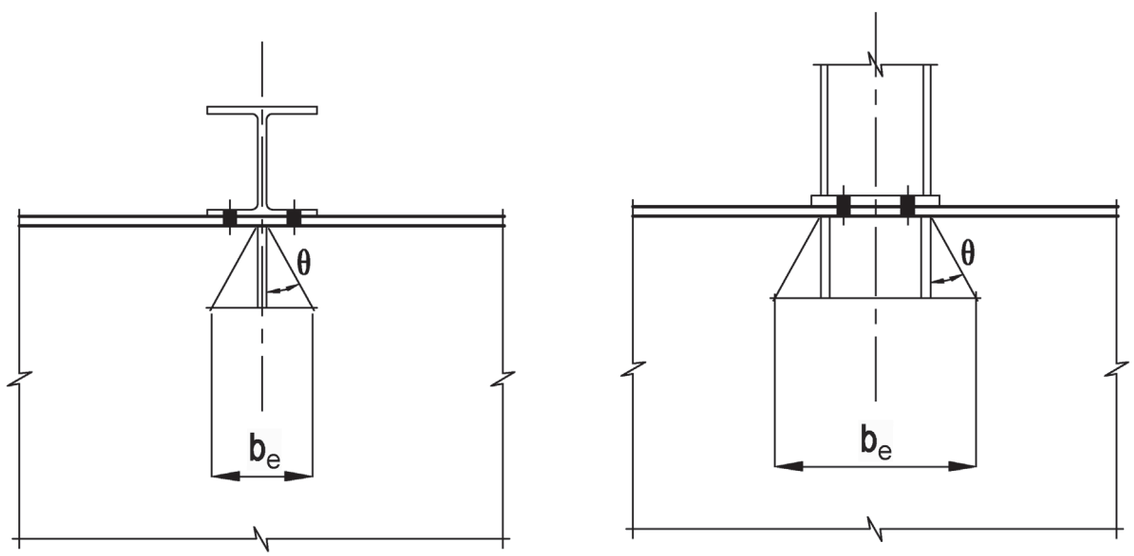

(a) *(b)*

Fig. 6. Detail for concentrated load at the roof of a tank or silo: (a) single stiffener; (b) multiple stiffeners.

stress trajectories, which are shown in Figure 9b. These plots confirmed the work of Wyss (1923) and Sandel (1950), showing that the maximum normal stress was at the end of the members and the stress trajectories were along approximately 30° lines with the connected member.

Irvan (1957) tested a model of a Pratt truss joint with double gusset plates. The gusset plates were ⅛-in.-thick aluminum, with a yield strength of 35 ksi and a modulus of elasticity of 10,000 ksi. Data from strain gauges were used to plot the tension, compression and shear stresses in the gusset plate. The stress trajectories are shown in Figure 9c. Although the plots show a slightly wider dispersion angle than those of Wyss (1923), Sandel (1950) and Whitmore (1952), Irvan proposed that the 30° lines should project from the center of gravity of the rivet group instead of the outside fasteners on the first row. This gives an effective stress trajectory angle of 16.1° over the full fastener length.

Chesson and Munse (1963) tested 30 riveted and bolted truss connections with gusset plates. The specimens were loaded in tension until one of the components failed. The authors recommended that the normal stress at the end of bracing members be calculated using a stress trajectory angle of 22° for plates with punched holes and 25° for plates with drilled holes.

Yamamoto, Akiyama and Okumura (1985) investigated the stress distribution of eight Warren- and Pratt-type truss joints with double gusset plates. Test specimens were made of 8-mm (0.315-in.)-thick gusset plates. They plotted the stress distribution using data from strain gauges mounted on the gusset plates. The researchers used the finite element method to perform an inelastic analysis on the plates. They found that "the plastic region, which appears in the inner part of the gusset plate at the earlier loading stage, develops toward the outer part with the load increasing." Using the results of "numerical evaluations of a great variety of bolt arrangements," the researchers proposed a dispersion angle of 22°.

Cheng and Grondin (1999) summarized the research on gusset plates loaded in compression at the University of Alberta. They noted that yielding in the specimens allowed the stress to redistribute and recommended a 45° dispersion angle. Using an equivalent column method to calculate the buckling strength with a 45° dispersion angle, the nominal strengths agreed well with the test results.

Additional research on gusset plates by Lavis (1967), Rabern (1983), Chakrabarti (1983), Bjorhovde and Chakrabarti (1985), Gross and Cheok (1988), and Girard, Picard and Fafard (1995) verified 30° stress trajectories.

Web Local Yielding

The equations for web local yielding in the 1937 AISC *Specification* (AISC, 1937) are based on a 45° dispersion angle from the load application point to the fillet, as shown in Figure 10. Based on nine tests of directly welded moment connections to column flanges, Sherbourne and Jensen (1957) showed that the 45° dispersion angle is overly conservative. They proposed a 63.4° dispersion angle (2-to-1 slope) for design.

Graham, Sherbourne, Khabbaz and Jensen (1959) tested 11 specimens that simulated the column near a compression flange in a directly welded moment connection. Yielding of the web initiated beneath the load, and the width of the yielded region became wider as the load increased. The specimens failed by buckling after significant yielding of the web. All of the test loads exceeded the nominal strength predicted using a dispersion angle of 74.0° (3.5-to-1 slope).

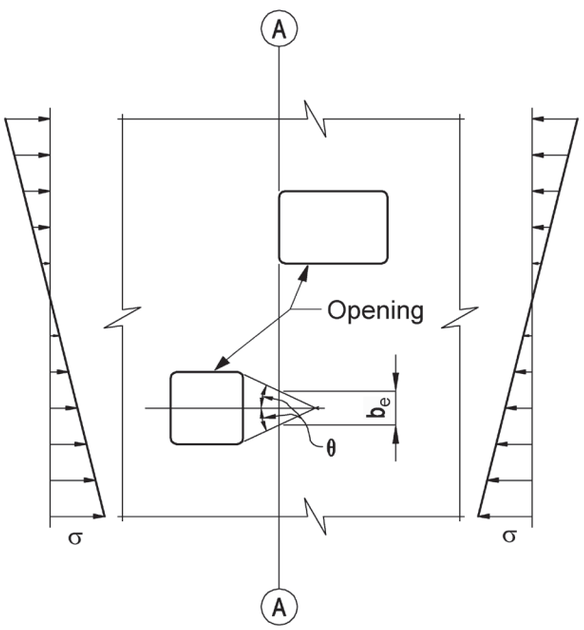

Fig. 7. Equivalent opening size.

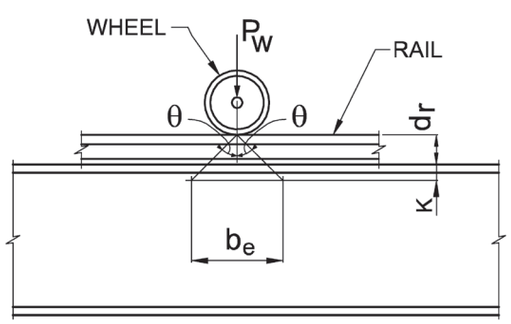

Fig. 8. Crane girder with a concentrated wheel load.

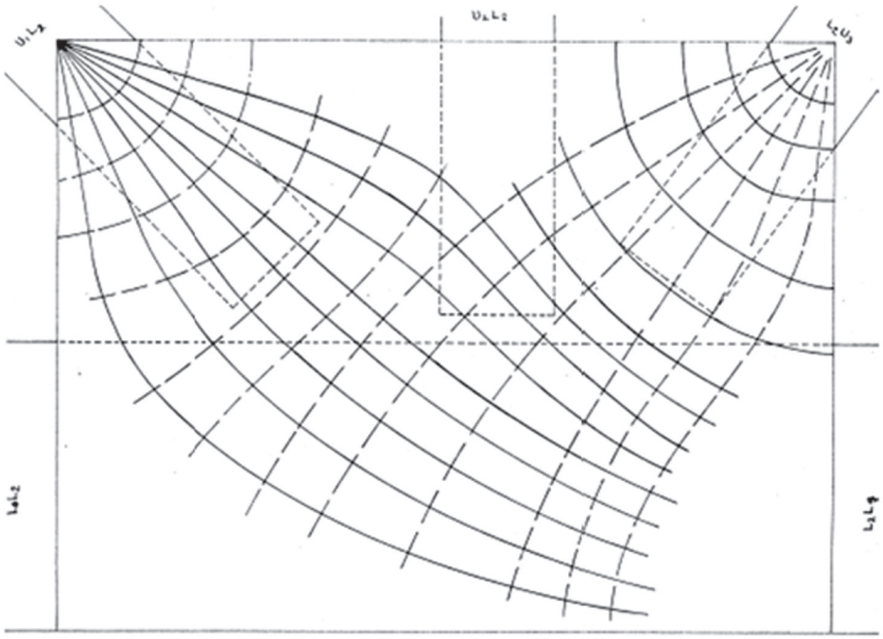

Fig. 9a. Experimental stress trajectories in gusset plates, Sandel (1950).

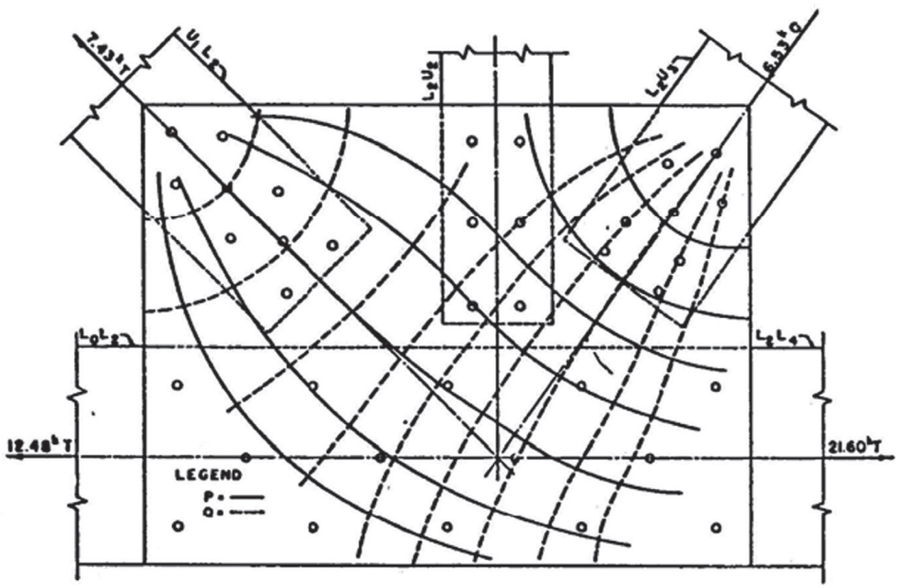

Fig. 9b. Experimental stress trajectories in gusset plates, Whitmore (1952).

The authors recommended a conservative dispersion angle of 68.2° (2.5-to-1 slope) for design purposes; however, they also presented a plastic analysis approach, where they recommended a dispersion angle of 74.0° (3.5-to-1 slope).

Based on experimental tests and numerical models, Aribert, Lauchal and Nawawy (1981) proposed three equations based on the magnitude of the load. At the maximum elastic load, they recommended an effective width of $t_p + 2.3k$, which is equivalent to a 26.6° dispersion angle through the end plate and a 49.0° dispersion angle through the column. At the maximum plastic load, they proposed an effective width of $2t_p + 5k$, which is equivalent to a 45° dispersion

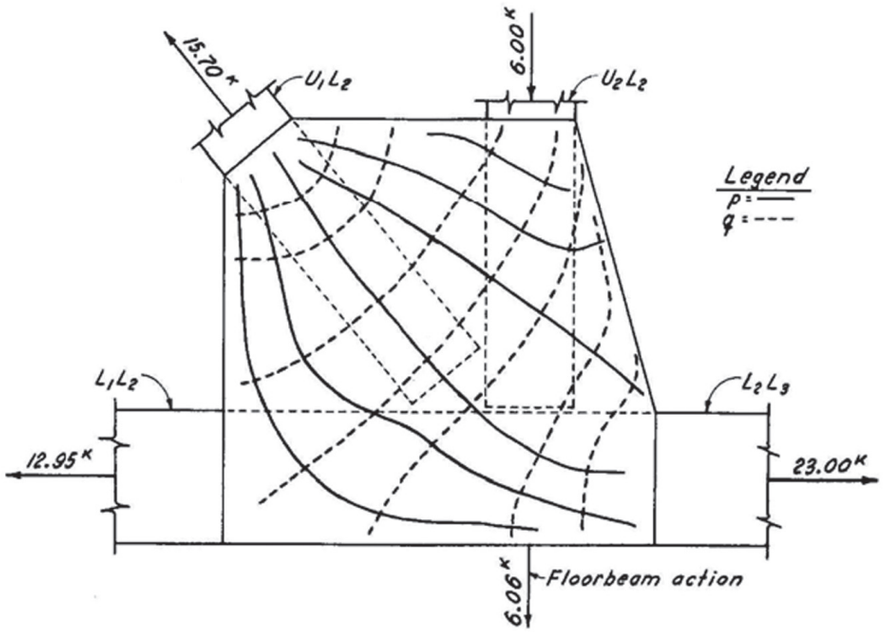

Fig. 9c. Experimental stress trajectories in gusset plates, Irvan (1957).

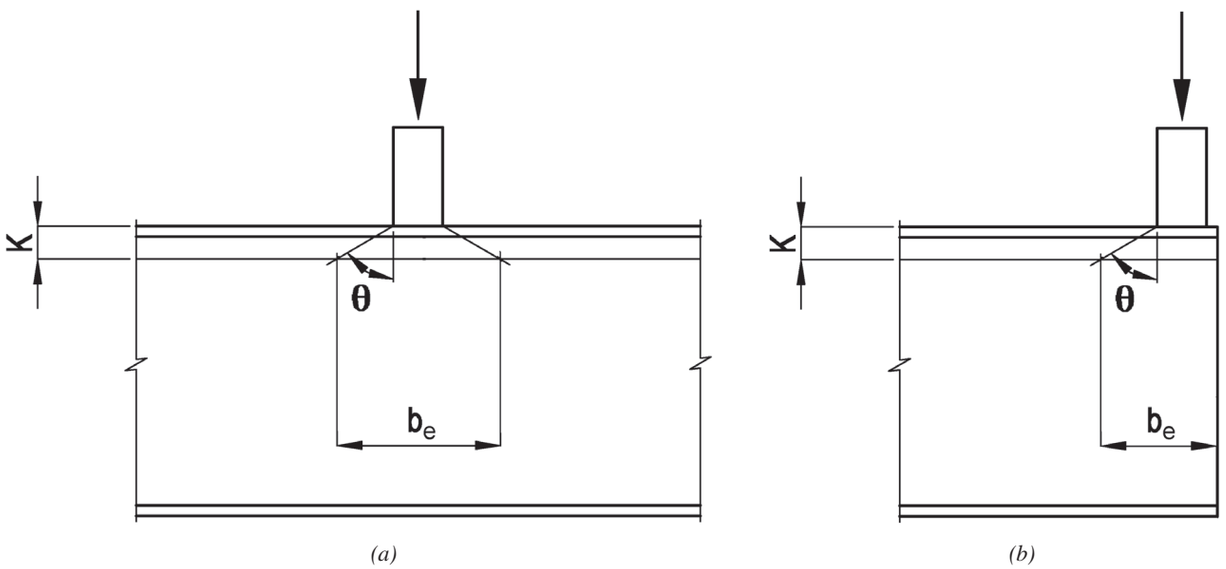

(a) *(b)*

Fig. 10. Effective width for web local yielding: (a) interior loading; (b) end loading.

angle through the end plate and a 68.2° dispersion angle through the column. At the ultimate load, the recommended effective width is $6t_p + 7k$, which is equivalent to a 71.6° dispersion angle through the end plate and a 74.0° dispersion angle through the column.

Based on inelastic finite element models and six experimental tests on end plate moment connections, Hendrick and Murray (1983) recommended a 45° dispersion angle through the weld and the end plate and a 71.6° dispersion angle (3-to-1 slope) through the column. These recommendations are also included in AISC Steel Design Guide 4 (Murray and Sumner, 2003). The tests and finite element models clearly showed that the dispersion angle increased with load, especially after the yield strain was exceeded.

Beam Webs

Young and Hancock (2000) tested a series of cold-formed channels with local compression loads in the plane of the web. They found that the dispersion angle through the web was greater for interior loading than for end loading. For members loaded at both flanges, the authors recommended dispersion angles of 54.5° and 31.0° for interior loading and end loading, respectively. For members loaded at only one flange, they recommended dispersion angles of 52.4° and 45.0° for interior loading and end loading, respectively.

Plate and Shell Structures

The finite element models of Wang (1974), Gould, Sen, Wang, Suryoutomo and Lowery (1976), and Zhao and Yu (2005) were used to study the behavior of discretely supported silos and tanks. As expected, the models showed that the compressive stress in the shell was much higher above the supports, and the buckling strength of the shell increased with the engagement length of the columns. Pasternak (2002) discussed two silos with discrete supports that failed in service due to local buckling of the shell directly above the support. He concluded that the stresses in the shell directly above the support were too high due to insufficient stiffener length.

Shear Lag

Abi-Saad and Bauer (2006) used an effective width approach with a dispersion angle of 30° to calculate the reduced strength of members due to the effects of shear lag.

General Observations

Young and Hancock (2000) showed that the element geometry affects the dispersion angle. When the member is loaded at the end, the average suggested dispersion angle is only 71% of the average value for interior loading.

The effect of constraint can be observed by comparing the gusset plate tests to the local web yielding tests. The test results showed dispersion angles of 22° to 45° for gusset plates and 49° to 74° for local web yielding. Gusset plates are plane stress elements, but the elements in local web yielding calculations are restrained by the beam flange in both directions perpendicular to the load.

Experimental observations of Graham et al. (1959), Aribert et al. (1981), Hendrick and Murray (1983), Yamamoto et al. (1985) and Cheng and Grondin (1999) showed that the stress dispersion angle increases with inelastic material behavior.

FRACTURE MECHANICS APPROACH

Fracture mechanics solutions are available for a wide range of loading conditions and crack geometries. Although cracks do not exist in the elements that are the subject of this paper, fracture mechanics can be used to determine the stress field adjacent to any discontinuity. The stress-trajectory angle around the discontinuity can be determined using the energy release rate of an equivalent crack.

Basic Solution

Bažant and Cedolin (1991) described a stress relief zone, which is a stress-free zone in the material ahead of a crack as shown in Figure 11. Their derivation, which used principles of fracture mechanics to determine the stress dissipation angle, is shown here. They assumed a region of zero stress to be bounded by lines of constant slope, k_s. The strain energy per unit thickness for a crack length $2a$ is

$$\Delta U = -2k_s a^2 u \tag{2}$$

The strain energy density is

$$u = \frac{\sigma^2}{2E} \tag{3}$$

The energy release rate on each side of the crack centerline is

$$W = \frac{-\mathrm{d}\Delta U}{\mathrm{d}a} = \frac{2k_s a \sigma^2}{E} \tag{4}$$

From Irwin (1957), the energy release rate per crack tip is

$$G = \frac{K_I^2}{E} \tag{5}$$

The critical stress intensity factor for a crack in an infinitely wide plate in tension is

$$K_I = \sigma\sqrt{\pi a} \tag{6}$$

Equation 6 is substituted into Equation 5 to get

$$G = \frac{\pi\sigma^2 a}{E} \tag{7}$$

Because W must equal G, Equation 4 is set equal to Equation 7 and solved for k_s. The slope of the stress dispersion line is

$$k_s = \frac{\pi}{2} \tag{8}$$

where

E = modulus of elasticity, ksi
G = energy release rate per crack tip, kip-in.
K_I = stress intensity factor, ksi-in.$^{1/2}$
ΔU = strain energy per unit thickness, kips
W = energy release rate on each side of the crack centerline, kip-in.
a = half crack length, in.
k_s = slope of the stress dispersion line
u = strain energy density, ksi
σ = applied axial stress, ksi

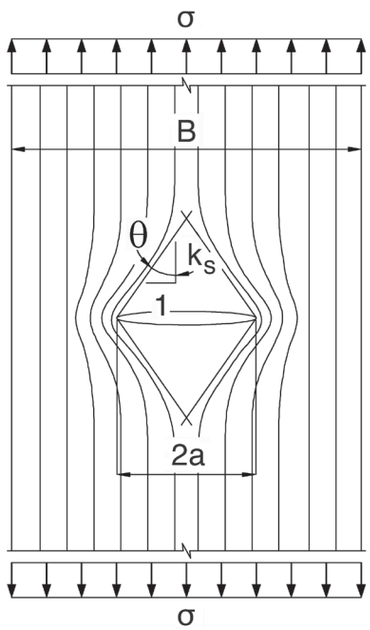

Fig. 11. Stress-free zone ahead of a crack.

This is equivalent to a dispersion angle of 32.5°, which is in reasonable agreement with the experimental results for elastic gusset plates. However, a general design solution must account for the element geometry, the effect of constraint and inelastic material behavior.

Effect of Element Geometry

The stress intensity factor is dependent on the element geometry, crack size, load level and loading configuration. In this paper, the elements will be loaded only in axial tension, and the only two element geometries will be considered: center crack tension (CCT) and single-edge notch tension (SENT). These are illustrated in Figure 12.

The stress intensity factor equations for cracks in infinitely wide plates are (Broek, 1986)

CCT

$$K_I = \sigma\sqrt{\pi a} \tag{9}$$

SENT

$$K_I = \beta\sigma\sqrt{\pi a} \tag{10}$$

where $\beta = 1.12$ is the free-surface correction factor.

Effect of Constraint

The strain energy density is the strain energy per unit volume, which is calculated as the area under the stress-strain curve. Equation 3 is applicable only to elastic materials in uniaxial tension. Cook and Young (1985) and Chen and Han (1988) showed the derivation of Equation 3.

$$\begin{aligned} u &= \int_0^{\varepsilon} \sigma d\varepsilon \\ &= \frac{\sigma\varepsilon}{2} \\ &= \frac{\sigma^2}{2E} \end{aligned} \tag{11}$$

For plane stress with no shear component, the strain energy density is

$$u = \int_0^{\varepsilon_{ij}} \sigma_{ij} d\varepsilon = \frac{1}{2E}\left(\sigma_x^2 + \sigma_y^2 - 2\upsilon\sigma_x\sigma_y\right) \quad (12)$$

And for three-dimensional stress with no shear component,

$$u = \int_0^{\varepsilon_{ij}} \sigma_{ij} d\varepsilon = \frac{1}{2E}\left[\sigma_x^2 + \sigma_y^2 + \sigma_z^2 - 2\upsilon\left(\sigma_x\sigma_y + \sigma_y\sigma_z + \sigma_z\sigma_x\right)\right] \quad (13)$$

where

ν = Poisson's ratio
ε_{ij} = strain tensor
σ_{ij} = stress tensor
σ_x = normal stress in the x direction, ksi
σ_y = normal stress in the y direction, ksi
σ_z = normal stress in the z direction, ksi

For states of stress with an applied load in the x-direction and constraint in the y- and z-directions, Blodgett (1998) derived Equations 14 and 15 to determine σ_y and σ_z normal stresses due to the constraint.

$$\sigma_y = \sigma_x (0.330C_y + 0.0989C_z) \quad (14)$$

$$\sigma_z = \sigma_x (0.0989C_y + 0.330C_z) \quad (15)$$

where

C_y = factor for restraint in the y-direction
C_z = factor for restraint in the z-direction

For plane stress conditions with an applied stress in the x-direction and rigid constraint in the y-direction, $C_y = 1.0$ and $C_z = 0$. When these values are substituted into Equations 14 and 15, the constraint stresses are

$$\sigma_y = 0.330\sigma_x \quad (16)$$

$$\sigma_z = 0.0989\sigma_x \quad (17)$$

If Equations 16 and 17 are substituted into Equation 13, with $\nu = 0.3$, the resulting strain energy density is

$$u = 0.421\frac{\sigma_x^2}{E} \quad (18)$$

For conditions with rigid constraint in the y- and z-directions, $C_y = 1.0$ and $C_z = 1.0$. When these values are substituted into Equations 14 and 15, the constraint stresses are

$$\sigma_y = 0.429\sigma_x \quad (19)$$

$$\sigma_z = 0.429\sigma_x \quad (20)$$

If Equations 19 and 20 are substituted into Equation 13, the resulting strain energy density is

$$u = 0.371\frac{\sigma_x^2}{E} \quad (21)$$

Another effect of the multi-axial state of stress is the higher effective yield stress of the material. Using von Mises' equation, the effective stress is (Boresi, Schmidt and Sidebottom, 1993).

$$\sigma_e = \sqrt{\frac{1}{2}\left[\left(\sigma_x - \sigma_y\right)^2 + \left(\sigma_y - \sigma_z\right)^2 + \left(\sigma_z - \sigma_x\right)^2\right]} \quad (22)$$

To determine the effective yield stress in the x-direction for conditions with rigid constraint in one direction, σ_y and σ_z from Equations 16 and 17 are substituted into Equation 22.

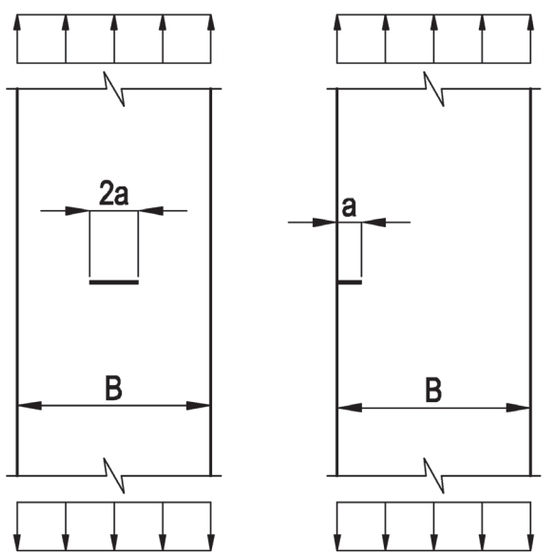

Fig. 12. Element geometry: (a) CCT; (b) SENT.

And then, Equation 22 is solved for σ_x. At yield, σ_e is equal to the uniaxial yield strength, F_y, and σ_x is equal to the effective yield stress in the x-direction, F'_y. These substitutions result in Equation 23.

$$F'_y = 1.23F_y \tag{23}$$

For rigid constraint in two directions, Equations 19 and 20 are substituted into Equation 22, which results in Equation 24.

$$F'_y = 1.75F_y \tag{24}$$

The x-direction strain is determined from Equation 25 (Cook and Young, 1985).

$$\varepsilon_x = \frac{1}{E}\left[\sigma_x - \upsilon\left(\sigma_y + \sigma_z\right)\right] \tag{25}$$

Equations 14 and 15 are substituted into Equation 25 to get Equation 26.

$$\varepsilon_x = \frac{\sigma_x}{E}\left[1 - 0.129\left(C_y + C_z\right)\right] \tag{26}$$

Inelastic Material Behavior

Based on linear-elastic perfectly plastic material behavior, the strain energy density for conditions of uniaxial stress with strains exceeding the yield strain is

$$u = F_y\left(\varepsilon - \frac{\varepsilon_y}{2}\right) \tag{27}$$

For multi-axial stress, the strain energy density is

$$u = F'_y\left(\varepsilon - \frac{\varepsilon'_y}{2}\right) \tag{28}$$

where

$$\varepsilon'_y = \frac{F'_y}{E}\left[1 - 0.129\left(C_y + C_z\right)\right] \tag{29}$$

ε_y = uniaxial yield strain
ε'_y = effective yield strain accounting for constraint

The stress intensity factor is a measure of the stress singularity at the crack tip. It is valid only in linear-elastic fracture mechanics (LEFM), which allows only small-scale yielding at the crack tip. Therefore, in the inelastic range, the accuracy of the LEFM solution degrades with increased inelasticity and elastic-plastic fracture mechanics (EPFM) must be used.

To estimate the effect of inelastic material behavior, Smith and Pilkington (1978) discussed the possibility of calculating a critical K_I value based on a J-integral solution, which was originally developed by Rice (1968) to characterize the fracture in nonlinear elastic materials. Elastic-plastic estimation procedures were developed by Shih and Hutchinson (1976), who proposed that the elastic-plastic J-integral value could be estimated as the sum of the elastic and plastic components:

$$J = J_e + J_p \tag{30}$$

The elastic value, J_e, is equal to Griffith's energy release rate, G (Griffith, 1920).

$$J_e = G \tag{31}$$

Irwin (1957) showed that, for conditions of plane stress,

$$\begin{aligned} G &= \frac{K_I^2}{E} \\ &= \frac{\pi\beta^2\sigma^2 a}{E} \end{aligned} \tag{32}$$

The value for K_I should be calculated with the effective crack size (Irwin, 1957), which is larger than the actual crack size due to the plastic zone adjacent to the crack tip. The modified Irwin plastic zone correction factor proposed by Kumar, German and Shih (1981) is

$$\begin{aligned} a_e &= a + \frac{1}{1 + \left(P/P_0\right)^2}\left(\frac{1}{2\pi}\right)\left(\frac{n-1}{n+1}\right)\left(\frac{K_I}{\sigma_0}\right)^2 \\ &= a\left[1 + \frac{\left(\sigma/\sigma_0\right)^2}{1 + \left(\sigma/\sigma_0\right)^2}\left(\frac{\beta^2}{2}\right)\left(\frac{n-1}{n+1}\right)\right] \end{aligned} \tag{33}$$

He and Hutchinson (1983) derived the fully plastic J-integral solution for semi-infinite plates with a crack at the center.

$$J_p = \pi\sqrt{n}\,\frac{k\varepsilon_0 a}{\sigma_0^n}\sigma^{n+1} \tag{34}$$

where n and k are Ramberg-Osgood coefficients (Ramberg and Osgood, 1943) for the true stress-strain curve. The Ramberg-Osgood equation is

$$\frac{\varepsilon}{\varepsilon_0} = \frac{\sigma}{\sigma_0} + k_r \left(\frac{\sigma}{\sigma_0} \right)^n \tag{35}$$

where σ_0 and ε_0 are usually set equal to the yield stress and yield strain, respectively. Variables n and k_r are determined empirically, based on the true stress-strain curve for the material in question. Values based on best-fit curve fitting to data in NIST (2005) are:

$k_r = 2.4$ and $n = 5.8$ for ASTM A36 steel
$k_r = 1.8$ and $n = 7.4$ for ASTM A572 Grade 50 steel

Equations 30 through 35 can be used to determine an effective J-integral solution; however, this results in a very complicated, iterative solution that can be simplified for design purposes into Equation 36.

$$J = \lambda G \tag{36}$$

where

$$\lambda = \frac{J_e + J_p}{J_e} \tag{37}$$

Although the J-integral solution is difficult to simplify into a reasonable design procedure, some general trends can be observed that will be used to formulate an empirical design expression for λ: J_e is directly proportional to σ^2 (see Equation 32) and J_p is directly proportional to σ^{n+1} (see Equation 34). Equation 38 accounts for these trends and appears to fit the experimental data reviewed in this paper. It is expected that refinements will be made as more data become available.

$$\lambda = 1 + 0.77\,(\alpha - 1) \tag{38}$$

where

$$\alpha = \frac{\varepsilon}{\varepsilon'_y} \tag{39}$$

DESIGN EQUATION

Derivation of Design Equation

Based on the fracture mechanics equations presented in this paper, a design equation will be derived that accounts for element geometry, constraint and inelastic material behavior. Equation 3 is combined with Equation 4 to get Equation 40.

$$W = 4k_s a u \tag{40}$$

Equation 28 can be expressed as

$$u = F'_y \varepsilon'_y \left(\alpha - \frac{1}{2} \right) \tag{41}$$

And Equation 29 can be expressed as

$$\varepsilon'_y = C_1 \frac{F'_y}{E} \tag{42}$$

where

$$C_1 = 1 - 0.129(C_y + C_z) \tag{43}$$

After substituting the proper values for C_y and C_z:
$C_1 = 1.00$ for uniaxial stress
$= 0.871$ for constraint in one direction
$= 0.742$ for constraint in two directions

Equations 23 and 24 can be expressed as

$$F'_y = C_2 F_y \tag{44}$$

where
$C_2 = 1.00$ for uniaxial stress
$= 1.23$ for constraint in one direction
$= 1.75$ for constraint in two directions

Equations 41, 42 and 44 are combined to get Equation 45.

$$u = C_1 C_2^2 \frac{F_y^2}{E} \left(\alpha - \frac{1}{2} \right) \tag{45}$$

Equation 45 is substituted into Equation 40 to get Equation 46.

$$W = 4k_s a C_1 C_2^2 \frac{F_y^2}{E} \left(\alpha - \frac{1}{2} \right) \tag{46}$$

Equation 5 is substituted into Equation 36 to get Equation 47.

$$J = \lambda \frac{K_I^2}{E} \tag{47}$$

W from Equation 46 is set equal to J from Equation 47 to get Equation 48.

$$\lambda K_I^2 = 4k_s a C_1 C_2^2 F_y^2 \left(\alpha - \frac{1}{2}\right) \tag{48}$$

Equation 10 is substituted into Equation 48 to get Equation 49.

$$\lambda \pi \beta^2 \sigma^2 = 4k_s C_1 C_2^2 F_y^2 \left(\alpha - \frac{1}{2}\right) \tag{49}$$

Equation 47 was derived for conditions of plane stress; therefore, for perfectly plastic materials, $\sigma = F_y$. Substituting for F_y simplifies Equation 49 to

$$\lambda \pi \beta^2 = 4k_s C_1 C_2^2 \left(\alpha - \frac{1}{2}\right) \tag{50}$$

To simplify the calculation, C_1 and C_2 can be combined into one variable:

$$C = C_1 C_2^2 \tag{51}$$

where

C = 1.00 for uniaxial stress
= 1.32 for constraint in one direction
= 2.27 for constraint in two directions

Equations 50 and 51 are combined to give Equation 52, which is recommended for design.

$$\tan\theta = \frac{1}{k_s} = \frac{4C\left(\alpha - \frac{1}{2}\right)}{\pi \lambda \beta^2} \tag{52}$$

General Trends of the Solution

Figure 13 shows the stress dispersion angle, θ, versus normalized strain, α, according to Equation 52. The general trends of the equation will now be discussed in relation to the behavior observed in the tests.

The effect of element geometry is accounted for in Equation 52 with the variable, β. For edge loading, the dispersion angle is reduced by $1/\beta^2 = 0.797$. The dispersion angles suggested by Young and Hancock (2000) show an average reduction of 0.710 for end-loaded members, which is a 12% difference between the test results and the proposed design procedure. Therefore, the general trend of Equation 52 is correct, but the accuracy is difficult to determine with the limited number of test results that are available.

The effect of constraint is accounted for with the variable, C. The effect of constraint can be observed by comparing the gusset plate tests to the web local yielding tests. Gusset plates are plane stress elements. For web local yielding, the element is restrained in two directions. In the existing research discussed in previous sections of this paper, dispersion angles of 22° to 45° were reported for gusset plates and 49° to 74° were reported for web local yielding. Figure 13 shows that the calculated dispersion angle increases with restraint; therefore, the general trend of Equation 52 is correct.

Inelastic material behavior is accounted for directly with α; however, the dispersion angle is also affected by λ, which varies with the level of inelasticity. Here, λ accounts for the difference between elastic fracture mechanics solution and the inelastic solution. Experimental observations of Graham et al. (1959), Aribert et al. (1981), Hendrick and Murray (1983), Yamamoto et al. (1985) and Cheng and Grondin (1999) showed that the stress dispersion angle increases with inelastic material behavior. This behavior is modeled well with Equation 52.

CALIBRATION OF ALPHA

It has been established that Equation 52 properly accounts for the variables affecting the dispersion angle. If the equation is to be used for design purposes, the level of inelasticity that can be tolerated must be established. Some elements must be designed essentially in the elastic range, such as

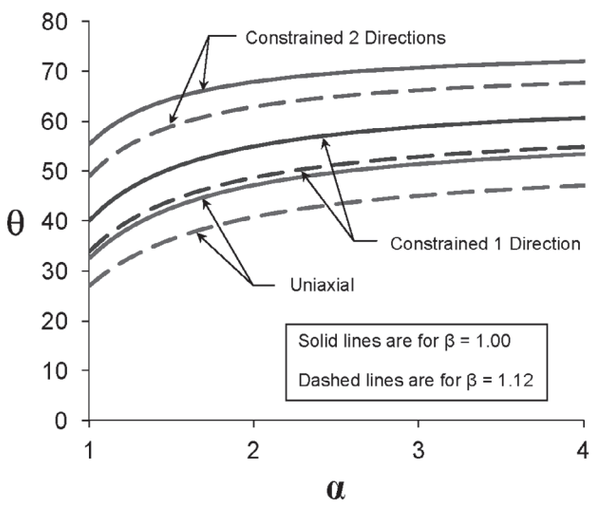

Fig. 13. Stress dispersion angle versus normalized strain.

slender elements susceptible to buckling and elements under high-fatigue cycles. If no inelastic action is expected, $\alpha = 1$. However, most elements in structural steel buildings can be designed under the assumption of at least some inelastic action. The design values for α will be selected to match existing test data reviewed in previous sections of this paper.

To provide reasonable agreement with the experimental results, a value of $\alpha = 1.7$ can be used for elements with adequate ductility to allow some inelastic deformation, but subject to stability problems after yielding. This includes elements such as gusset plates and beam webs. So, $\alpha = 3.8$ can be used for elements with adequate ductility to allow inelastic deformation without the possibility of buckling. This commonly occurs where the load is dispersed through a beam flange and *k*-distance for local web yielding calculations. Here, $\alpha = 10$ can be used for elements with adequate ductility to allow large inelastic deformations without the possibility of buckling. This is recommended for ultimate strength calculations. Table 1 lists the dispersion angles for all combinations with $\beta = 1$ and 1.12; $\alpha = 1.0$, 1.7, 3.8 and 10; and the three conditions of restraint discussed in this paper.

Gusset Plates

The early research on gusset plates focused on elastic stress distribution, and the proposed dispersion angle of 30° has been adopted in design; however, more recent studies by Cheng and Grondin (1999) showed that dispersion angles of 45° can be used if some inelasticity is tolerable. The proposed design procedure using $\beta = 1.00$ and $C = 1.00$ predicts 32.5° for plates with no inelastic capacity and 44.8° for inelastic design with $\alpha = 1.7$.

For conditions wherein the effective width extends beyond the plate boundaries as shown in Figure 14, $\beta = 1.12$ may be appropriate, although the test results are inconclusive for this type of plate geometry. For $C = 1.00$, the dispersion angle is 26.9° for plates with no inelastic capacity and 38.4° for inelastic design with $\alpha = 1.7$.

Web Local Yielding

There is an abundance of test data at various levels of inelasticity to calibrate α for local web yielding calculations, where the stress disperses through the *k*-distance of the beam (θ_1 in Figure 15). For interior loads, $\beta = 1.00$ and the element is constrained by the flange in two directions, which gives calculated values of $\theta = 55.3°$ when $\alpha = 1.0$, $\theta = 71.7°$ when $\alpha = 3.8$, and $\theta = 73.9°$ when $\alpha = 10$.

For elastic load levels, Aribert et al. (1981) proposed a dispersion angle of 49.0°, which is more conservative than the 55.3° angle calculated with Equation 52 at $\alpha = 1.0$.

For design load levels where some inelastic deformation can be accommodated, Sherbourne and Jensen (1957) proposed a 63.4° dispersion angle. Graham et al. (1959) and Aribert et al. (1981) suggested a value of 68.2°, and Hendrick and Murray (1983) recommended 71.6°. All of these empirical dispersion angles fall between the values calculated with $\alpha = 1.0$ and $\alpha = 3.8$; however, the 71.6° angle suggested by Hendrick and Murray (1983) is essentially equal to the calculated value of 71.7° with $\alpha = 3.8$.

At ultimate loads, Graham et al. (1959), and Aribert et al. (1981) proposed a value of 74.0°, which agrees well with the 73.9° angle calculated with $\alpha = 10$.

For conditions wherein the concentrated load is near the end of the member as shown in Figure 16, $\beta = 1.12$ may be appropriate. For $C = 2.27$, the dispersion angle is 49.0° for elements with no inelastic capacity and 67.5° for inelastic design with $\alpha = 3.8$.

Beam Webs

The tests by Young and Hancock (2000) on cold-formed channels reveal some information regarding the dispersion angle through beam webs, shown as θ_2 in Figure 15. Although the value of α is difficult to determine for the experiments, the inelastic capacity is expected to be minimal due to stability problems associated with the thin-walled channels that were tested. At interior loads, they suggested an average dispersion angle of 53.5°, which is much greater than 40.4°, the elastic value for θ calculated with $\beta = 1.00$ and $C = 1.32$ (constrained in one direction). The test results agree better with Equation 52 with $\alpha = 1.7$, which gives $\theta = 52.7°$.

At end loads, Young and Hancock (2000) suggested an average angle of 38.0°, which falls between the calculated values of 33.8° when $\alpha = 1.0$ and 46.3° when $\alpha = 1.7$. These angles were calculated with $\beta = 1.12$ and $C = 1.32$.

Crane Beams

For the crane beam in Figure 8, the dispersion angle through the rail and top flange can be calculated assuming constraint

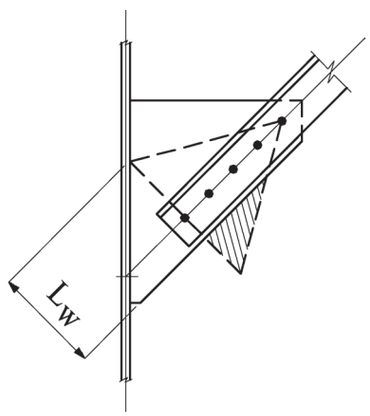

Fig. 14. Effective width beyond the plate boundaries.

Table 1. Dispersion Angles			
β	α	Constraint	θ (degrees)
1.00	1.0	no constraint	32.5
		one direction	40.4
		two directions	55.3
	1.7	no constraint	44.8
		one direction	52.7
		two directions	66.1
	3.8	no constraint	53.1
		one direction	60.4
		two directions	71.7
	10	no constraint	56.8
		one direction	63.6
		two directions	73.9
1.12	1.0	no constraint	26.9
		one direction	33.8
		two directions	49.0
	1.7	no constraint	38.4
		one direction	46.3
		two directions	60.9
	3.8	no constraint	46.7
		one direction	54.5
		two directions	67.5
	10	no constraint	50.6
		one direction	58.1
		two directions	70.1

in two directions with $\beta = 1.00$, which gives $\theta = 55.3°$ for $\alpha = 1.00$. This is less than the value of 60° suggested by Ricker (1982), but shows that the value of 45° adopted in CMAA (1994), AS (2001) and AISE (1997) is overly conservative.

Welded Plate

For connections with a plate welded to the flange of a member as shown in Figure 17, the flange can be considered constrained in two directions, and the effective width of the plate can be calculated with a dispersion angle of 55.3° for plates with no inelastic capacity and 71.7° for inelastic design with $\alpha = 3.8$.

PROPOSED DESIGN PROCEDURE

An appropriate design value for the stress dispersion angle, θ, can be calculated with the following design procedure:

- Select an appropriate value for α based on the inelastic capacity (see Table 2).
- Calculate λ with Equation 38.

$$\lambda = 1 + 0.77(\alpha - 1) \tag{38}$$

- Determine the constraint factor, *C*.
  C = 1.00 for uniaxial stress
  = 1.32 for constraint in one direction
  = 2.27 for constraint in two directions
- Determine the geometry factor, β.
  Under normal conditions, $\beta = 1.00$
  If the effective width extends beyond the edge of the element as shown in Figures 14 and 16, $\beta = 1.12$

Table 2. Design Values for α		
α	**Inelastic Capacity**	**Examples**
1.0	essentially elastic	slender elements elements with high fatigue cycles
1.7	some inelastic deformation with potential for inelastic buckling	gusset plates beam webs
3.8	some inelastic deformation—no buckling	local web yielding
10	large inelastic deformation—no buckling	ultimate strength calculations

- Calculate θ with Equation 52.

$$= \frac{4C\left(\alpha - \frac{1}{2}\right)}{\pi\lambda\beta^2} \tag{52}$$

CONCLUSIONS

The existing literature contains a wide range of recommended dispersion angles for stress flow around discontinuities in steel structures. Therefore, it is important to determine the variables affecting the stress flow so that the proper dispersion angles can be used in design.

Using fracture mechanics, it was shown that the dispersion angle is dependent on geometry, constraint and inelastic deformation capacity. An analytical model was derived that accounts for all variables affecting the dispersion angle. The model was shown to properly predict the experimental trends. A versatile design procedure, which explicitly accounts for all variables affecting the stress dissipation angle, was presented. Because the design variables related to the inelastic capacity were calibrated to the test results, the proposed design values agree well with the experimental values.

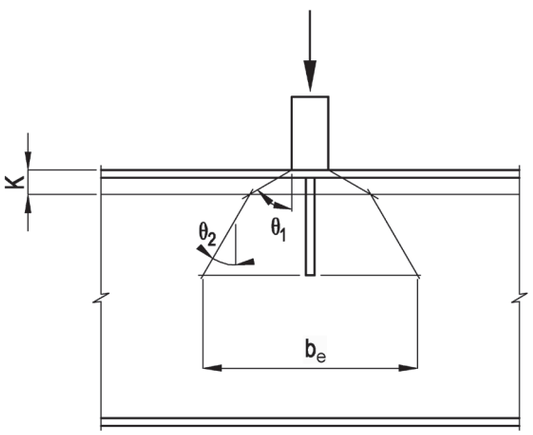

Fig. 15. Effective width of a beam web subjected to a concentrated load.

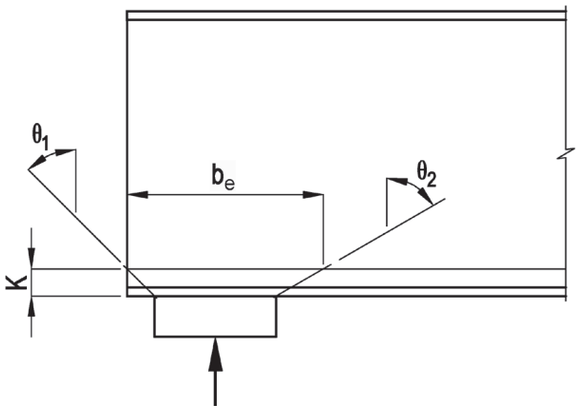

Fig. 16. Effective width of a beam web subjected to a concentrated end load.

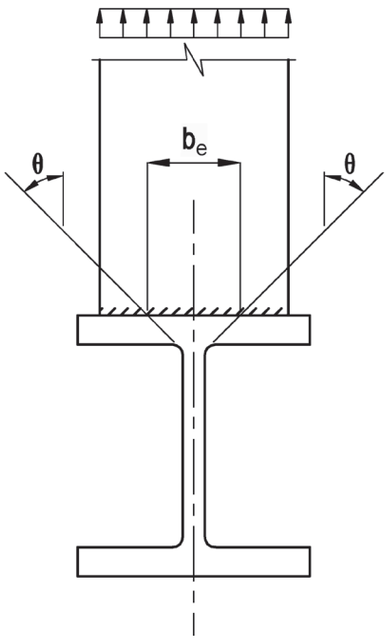

Fig. 17. Effective width of a plate welded to a column flange.

REFERENCES

Abi-Saad, G. and Bauer, D. (2006), "Analytical Approach for Shear Lag in Welded Tension Members," *Canadian Journal of Civil Engineering*, Vol. 33, pp. 384–394.

ABS (2009), *Common Structural Rules for Double Hull Oil Tankers*, American Bureau of Shipping, July.

AISC (1937), *Specification for the Design, Fabrication and Erection of Structural Steel for Buildings*, American Institute of Steel Construction, New York, NY.

AISC (2010), *Specification for Structural Steel Buildings*, June 22, American Institute of Steel Construction, Chicago, IL.

AISC (2011), *Steel Construction Manual*, 14th ed., American Institute of Steel Construction, Chicago, IL.

AISE (1997), *Guide for the Design and Construction of Mill Buildings*, AISE Technical Report No. 13, Association of Iron and Steel Engineers.

Aribert, J.M., Lauchal, A. and Nawawy, O.I. (1981), "Elastic-Plastic Modelization of the Resistance of a Column Web in the Compression Region," *Construction Métallique*, No. 2, June.

AS (2001), *Cranes, Hoists and Winches, Part 18: Crane Runways and Monorails*, Australian Standard, AS 1418.18.

ASME (2001), *Steel Stacks*, ASME STS-1-2000, American Society of Mechanical Engineers.

Bažant, Z.P. and Cedolin, L. (1991), *Stability of Structures, Elastic, Inelastic, Fracture, and Damage Theories*, Oxford University Press, New York, NY.

Bjorhovde, R. and Chakrabarti, S.K. (1985), "Tests of Full-size Gusset Plate Connections," *Journal of Structural Engineering,* ASCE, Vol. 111, No. 3, pp. 667–683.

Blodgett, O.W. (1998), "The Effect of Constraint on Ductility in Welded Beam-to-Column Connections," Seminar notes from the seminar*, Design of Welded Structures,* by the Lincoln Electric Company.

Boresi, A.P., Schmidt, R.J. and Sidebottom, O.M. (1993), *Advanced Mechanics of Materials*, 5th ed., John Wiley and Sons, New York, NY.

Broek, D. (1986), *Elementary Engineering Fracture Mechanics*, 4th ed., Kluwer Academic Publishers.

Chakrabarti, S.K. (1983), *Tests of Gusset Plate Connections,* M.S. Thesis, University of Arizona, Tucson, AZ.

Chen, W.F. and Han, D. (1988), *Plasticity for Structural Engineers*, Springer-Verlag, New York, NY.

Cheng, J.J.R. and Grondin, G.Y. (1999), "Recent Development in the Behavior of Cyclically Loaded Gusset Plate Connections," *Proceedings, North America Steel Construction Conference*. American Institute of Steel Construction, Chicago, IL, pp. 8-1 – 8-22.

Chesson, E. and Munse, W.H. (1963), "Riveted and Bolted Joints: Truss-Type Tensile Connections," *Journal of the Structural Division, Proceedings of the American Society of Civil Engineers,* Vol. 89, No. ST1, February, pp. 67–106.

CICIND (1999), *Model Code for Steel Chimneys*, Revision 1, Hertfordshire, UK.

CMAA (1994), *Specifications for Top Running Bridge and Gantry Type Multiple Girder Electric Overhead Traveling Cranes*, Specification 70, Crane Manufacturers Association of America.

Cook, R.D. and Young, W.C. (1985), *Advanced Mechanics of Materials*, Macmillan Publishing Company, New York, NY.

Eurocode (2005), Eurocode 3: Design of Steel Structures—Part 1-8: Design of Joints, European Standard, EN 1993-1-8.

Girard, C., Picard, A. and Fafard, M. (1995), "Finite Element Modeling of the Shear Lag Effects in an HSS Welded to a Gusset Plate," *Canadian Journal of Civil Engineering,* Vol. 22, pp. 651–659.

Gould, P.L., Sen, S.K., Wang, R.S.C., Suryoutomo, H. and Lowery, R.D. (1976), "Column Supported Cylindrical-Conical Tanks," *Journal of the Structural Division*, Vol. 102, No. ST2, February, pp. 429–447.

Graham, J.D., Sherbourne, A.N., Khabbaz, R.N. and Jensen, C.D. (1959), *Welded Interior Beam-to-Column Connections*, American Institute of Steel Construction, Chicago, IL.

Griffith, A.A. (1920), "The Phenomena of Rupture and Flow in Solids," *Philosophical Transactions of the Royal Society of London*, Series A, Vol. 221, pp. 163–198.

Gross, J.L. and Cheok, G. (1988), *Experimental Study of Gusseted Connections for Laterally Braced Steel Buildings,* National Institute of Standards and Technology, Gaithersburg, MD, November.

He, M.Y. and Hutchinson, J.W. (1983), "Fully-Plastic J-Solutions for Cracks in Infinite Solids," *Elastic-Plastic Fracture, Second Symposium,* Vol. 1, ASTM STP 803, American Society for Testing and Materials.

Hendrick, A. and Murray, T.M. (1983), "Column Web and Flange Strength at End-Plate Connections," Report FSEL/AISC 83-01, School of Civil Engineering and Environmental Science, University of Oklahoma.

Irvan, W.G. (1957), "Experimental Study of Primary Stresses in Gusset Plates of a Double Plane Pratt Truss," University of Kentucky Engineering Research Station Bulletin No. 46, December.

Irwin, G.R. (1957), "Analyses of Stresses and Strains Near the End of a Crack Traversing a Plate," *Journal of Applied Mechanics*, ASME, Vol. 24, pp. 361–364.

Kaups, T. and Lieb, J.M., (1986), "A Practical Guide for the Design of Quality Bulk Storage Bins and Silos," *International Journal of Bulk Solids Storage in Silos*, Vol. 2, No. 2, pp. 9–24.

Kumar, V., German, M.D. and Shih, C.F. (1981), "An Engineering Approach for Elastic-Plastic Fracture Analysis," EPRI Report NP-1931, Electric Power Research Institute, Palo Alto, CA, July.

Lavis, C.S. (1967), *Computer Analysis of the Stresses in a Gusset Plate*, Master's Thesis, University of Washington, Seattle, WA.

Murray, T.M. and Sumner, E.A. (2003), *Extended End-Plate Moment Connections, Seismic and Wind Applications*, Steel Design Guide 4, 2nd ed., American Institute of Steel Construction, Chicago, IL.

NIST (2005), *Mechanical Properties of Structural Steels*, Federal Building and Fire Safety Investigation of the World Trade Center Disaster, U.S. Department of Commerce, September.

Owens, G.W. and Cheal, B.D. (1989), *Structural Steelwork Connections*, Butterworths, London, UK.

Pasternak, H. (2002), "Silos and Tanks," *Refurbishment of Buildings and Bridges*, CISM Course 435, Chapter 3, edited by Mazzolani, F.M. and Ivanyi, M., Springer, pp. 166–180.

Rabern, D.A. (1983), *Stress, Strain and Force Distributions in Gusset Plate Connections*, Master's Thesis, University of Arizona, Tucson, AZ.

Ramberg, W. and Osgood, W.R. (1943), "Description of Stress-Strain Curves by Three Parameters," Technical Note 902, National Advisory Committee for Aeronautics, July.

Rice, J.R. (1968), "A Path-Independent Integral and the Approximate Analysis of Strain Concentration by Notches and Cracks," *Journal of Applied Mechanics*, ASME, Vol. 35, pp. 379–386.

Ricker, D.T. (1982), "Tips for Avoiding Crane Runway Problems," *Engineering Journal*, American Institute of Steel Construction, Vol. 19, No. 4, Fourth Quarter.

Sandel, J.A. (1950), *Photoelastic Analysis of Gusset Plates*, Master's Thesis, University of Tennessee, Knoxville, TN, December.

Sherbourne, A.N. and Jensen, C.D. (1957), *Direct Welded Beam Column Connections*, Report No. 233.12, Fritz Laboratory, Lehigh University, Bethlehem, PA.

Shih, C.F. and Hutchinson, J.W. (1976), "Fully Plastic Solutions and Large-Scale Yielding Estimates for Plane Stress Crack Problems," *Journal of Engineering Materials and Technology*, Vol. 98, pp. 289–295.

Smith, E. and Pilkington, R. (1978), "The Characterization of Crack-Tip Deformation Fields in Non-Linear Materials," *Non-Linear Problems in Stress Analysis*, P. Stanley, ed., Applied Science Publishers.

Wang, S. (1974), *Design of Cylindrical Steel Tanks Subjected to Concentrated Support Loads*, Ph.D. Dissertation, Washington University, St. Louis, MO, December.

Whitmore, R.E. (1952), "Experimental Investigation of Stresses in Gusset Plates," University of Tennessee Engineering Experiment Station Bulletin No. 16, May.

Wolf, C.D. (1983), "Structural Design Aspects of Materials Handling Plant," *Metal Structures Conference*, *Proceedings,* Brisbane, Australia, The Institution of Engineers, May, pp. 148–158.

Wozniak, R.S. (1990), "Steel Tanks," *Structural Engineering Handbook*, 3rd ed., Section 27, E.H. Gaylord and C.N. Gaylord, eds., McGraw-Hill, New York, NY.

Wyss, T. (1923), "Die Kraftfelder in Festen Elastischen Korpern und ihre Praktischen Anwendungen," Berlin, Germany (in German).

Yamamoto, K., Akiyama, N. and Okumara, T. (1985), "Elastic Analysis of Gusseted Truss Joints," *Journal of Structural Engineering,* ASCE, Vol. 111, No. 12, December, pp. 2545–2564.

Young, B. and Hancock, G.J. (2000), "Tests and Design of Cold-Formed Unlipped Channels Subjected to Web Crippling," *Proceedings of the Fifteenth International Specialty Conference on Cold-Formed Steel Structures*, St. Louis, MO, October 19–20, pp. 43–70.

Zhao, Y. and Yu, J. (2005), "Stability Behavior of Column-Supported Steel Silos with Engaged Columns," *Advances in Steel Structures*, *Proceedings of the Fourth International Conference,* edited by Shen, Z.Y., Li, G.Q. and Chan, S.L., June.